





Probing missing physics from inspiralling compact binaries via time-frequency tracks

Debtroy Das ¹, Soumen Roy ^{2,3}, Anand S. Sengupta ⁴ and Cosimo Bambi ^{1,5}

¹*Center for Astronomy and Astrophysics, Center for Field Theory and Particle Physics, and Department of Physics, Fudan University, Shanghai 200438, China.*

²*Centre for Cosmology, Particle Physics and Phenomenology - CP3, Université Catholique de Louvain, Louvain-La-Neuve, B-1348, Belgium.*

³*Royal Observatory of Belgium, Avenue Circulaire, 3, 1180 Uccle, Belgium.*

⁴*Department of Physics, Indian Institute of Technology Gandhinagar, Gujarat 382055, India.*

⁵*School of Natural Sciences and Humanities, New Uzbekistan University, Tashkent 100007, Uzbekistan.*

(Dated: July 30, 2025)

The orbital evolution of binary black hole (BBH) systems is determined by the component masses and spins of the black holes and the governing gravity theory. Gravitational wave (GW) signals from the evolution of BBH orbits offer an unparalleled opportunity for examining the predictions of General Relativity (GR) and for searching for missing physics in the current waveform models. We present a method of stacking up the time-frequency pixel energies through the orbital frequency evolution with the flexibility of gradually shifting the orbital frequency curve along the frequency axis. We observe a distinct energy peak corresponding to the GW signal's quadrupole mode. If an alternative theory of gravity is considered and the analysis of the BBH orbital evolution is executed following GR, the energy distribution on the time-frequency plane will be significantly different. We propose a new consistency test to check whether our theoretical waveform explains the BBH orbital evolution. Through the numerical simulation of beyond-GR theory of gravity and utilizing the framework of second-generation interferometers, we demonstrate the efficiency of this new method in detecting any possible departure from GR. Finally, when applied to an eccentric BBH system and GW190814, which shows the signatures of higher-order multipoles, our method provides an exquisite probe of missing physics in the GR waveform models.

I. INTRODUCTION

General relativity (GR) is the modern foundation of physics that explains gravitational interactions and spacetime geometry. The direct detection of gravitational waves (GWs) from compact binary coalescences [1–4] by Advanced LIGO [5] and Advanced Virgo [6] has led to tremendous progress in exploring the tests of GR in the strong and dynamic regime over the past ten years [7–11]. The approaches for testing GR can be broadly categorized into theory-specific and theory-agnostic tests [12]. The former approach involves analyzing GW signals through the lens of both GR and alternative gravity theories, aiming to identify either a model better interprets the data or constrain parameters within the alternative theory that reduce to GR under certain conditions. Conversely, the latter approach focuses on identifying potential deviations from predictions based solely on GR. Theories beyond GR may introduce modifications to standard predictions by altering the gravitational field of BHs, the generation of GWs, and the propagation of signals [13–18].

Since waveform models in alternative theories of gravity are not yet sufficiently developed to enable rigorous tests, and the true underlying theory may still be unknown, several null tests have been proposed to detect deviations

from the predictions of GR. Although these null tests offer valuable ways to probe deviations from GR, most of them rely on parameterized modifications in the phase evolution of GWs, either during the inspiral phase [19–27] or in the merger-ringdown phase [22, 28–32]. The statistical bounds on the parametrized deviations from GR depend on the assumptions and systematic errors of GW modeling [33–38].

On the other hand, the importance of signal assumption is low for consistency tests, such as the residual analysis. This method investigates whether any signal remains after subtracting the best-fit GR waveform from the data [7]. We search for coherent residuals across detectors using the BAYESWAVE framework [39], which employs a set of Morlet wavelets. Due to its broad parameter space, the method has significant flexibility in identifying residual features as coherent signals. As a result, its sensitivity to deviations from GR is reduced unless those deviations are loud.

Another complementary method for testing consistency is evaluating the agreement between the reconstructed signal and the posterior waveform samples obtained from parameter estimation [40]. The reconstructed signal is typically obtained using the unmodeled frameworks such as CWB [41, 42] and BAYESWAVE [39], which reconstruct

any coherent features in the data across the detector network. Recently, a semi-modeled approach has been introduced to reconstruct the signal [43]. Instead of searching for coherent features, it uses the posterior waveforms to identify essential wavelets that can represent the signal more efficiently. These methods are sensitive to detecting deviations from GR or missing physics in the theoretical waveform model. However, the accuracy of the reconstruction strongly depends on the chirp mass, as the overlap at a fixed signal-to-noise ratio decreases with a lower chirp mass [43].

In this work, we aim to develop a new consistency test that leverages the information contained in the orbital evolution. This approach is particularly sensitive to low-to-moderate mass binaries, where the long inspiral phase enhances our ability to detect deviations in dynamics. The orbital evolution of BBH systems serves as a pristine laboratory for testing GR and searching for signatures of new physics. The fidelity with which current waveform models reproduce the true inspiral dynamics remains contingent on the assumption that GR is the correct theory of gravity. If this assumption is violated, the inferred orbital dynamics will deviate from the GR-predicted behavior [44]. For instance, dipole radiation in modified gravity theories forces binaries to inspiral more rapidly, leading to faster GW chirps [45]. Even within the regime of GR, additional physical effects—such as the orbital hangup effect [46, 47], orbital eccentricity, spin precession [48, 49] or environmental influences including dynamical friction or accretion from a surrounding medium [50–52]—can alter the orbital evolution of BBHs. Hence, the energy distribution of the GW signal on the time-frequency plane is expected to exhibit systematic differences compared to our baseline GR-based model.

We introduce a novel theory-agnostic approach to consistency testing by directly analyzing the orbital frequency evolution of compact binaries on the time-frequency plane. Our method begins with Bayesian parameter estimation for a given signal, from which we extract the orbital frequency trajectory for each posterior sample. We then stack the time-frequency pixel energies along this trajectory, applying a flexible shift along the frequency axis. This effectively allows us to track the signal’s orbital evolution while remaining agnostic to any specific GW model.

To demonstrate the efficiency of our method, we analyze a signal that contains the non-GR effects due to a massive graviton. After that, we conduct consistency tests on signals generated from numerical simulations of an eccentric binary, while the search template waveform assumes a quasi-circular orbit. Finally, we apply to real data from the GW190814 event [53], which indicates

the presence of higher multipole modes. Although this method is conceptually straightforward, it is sensitive to cumulative mismatches in the signal that arise from incorrect assumptions about the underlying gravitational theory.

A key advantage of this method is its independence from predefined models. It allows researchers to explore beyond-GR effects and potential waveform modeling uncertainties within GR frameworks. In contrast to traditional template-based or parametrized tests, our method directly probes the signal’s energy distribution in the time-frequency plane. This makes it particularly well-suited for situations where reliable theoretical waveforms are unavailable, offering a flexible and powerful tool for detecting deviations from GR and identifying missing physics in the inspiral phase of compact binary coalescences.

The manuscript is compiled as follows. Section II describes the methodology of our consistency test. We do a brief literature review that inspired our work and assemble the data analysis and mathematical tools to postulate the consistency test. Furthermore, we build the required statistics needed to verify our findings. In Section III, we exhibit the validity of our methodology with a case study. We then demonstrate another case study by analyzing GW190814 data in Section IV. The paper ends with a concluding summary and discussion in Section V.

II. METHODOLOGICAL FRAMEWORK

This section outlines the methodology of our study, which consists of three main components. The first component involves extracting frequency evolution information from the inspiral phase of GW signals utilizing high-resolution time-frequency representations (TFRs). The second component focuses on developing a consistency test that compares the observed dynamics of BBH systems to the predictions derived from GR. Lastly, the third component establishes the statistical validation for this test, analyzing GR-based signals in the presence of stationary Gaussian noise.

Our methodology demonstrates that any systematic deviations from the expected outcomes may indicate the necessity for new physics, potentially introducing additional degrees of freedom in the theory of gravity or exposing shortcomings in the GW model within the context of GR. We quantify these departures to determine whether we have overlooked any necessary physical effects in the baseline waveform model.

A. Analysis of Time-Frequency Representation

Previous studies have utilized the TFRs of BBH mergers to identify higher-order multipoles in the inspiral part of the signals [54]. This approach has been extensively employed by the LVK Collaboration to detect higher multipole radiation present in the GW190412 signal [55] and subsequently found strong evidence from the GW190814 signal [53].

During the inspiral phase of a binary system, the instantaneous frequency $f_{\ell m}(t, \vec{\lambda})$ of a spherical harmonic mode (ℓ, m) is approximately related to the orbital frequency $f_{\text{orbital}}(t, \vec{\lambda})$ as $f_{\ell m}(t, \vec{\lambda}) \approx m f_{\text{orbital}}(t, \vec{\lambda})$, where $\vec{\lambda}$ represents the set of binary parameters. The dominant gravitational-wave mode corresponds to $(\ell, m) = (2, 2)$, and the prominent “hot pixels” in the TFR trace this same frequency evolution.

To extract energy distributions in the TFR, we define an arbitrary frequency track by scaling the orbital frequency:

$$f_{\alpha}(t, \vec{\lambda}) = \alpha f_{\text{orbital}}(t, \vec{\lambda}), \quad (1)$$

where α is a positive scaling factor. We scan α over a discrete range $[\alpha_{\min}, \alpha_{\max}]$. For each value of α , we compute the energy along the corresponding frequency track by summing time-frequency pixels along the $f_{\alpha}(t, \vec{\lambda})$:

$$S(\alpha) = \sum_{t_{\text{ISCO}} - \Delta t}^{t_{\text{ISCO}}} \left| \tilde{X}(t, f = f_{\alpha}(t, \vec{\lambda})) \right|^2, \quad (2)$$

where $\tilde{X}(t, f)$ is the TFR of the GW signal obtained by performing continuous wavelet transformation (CWT). The quantity t_{ISCO} is the time at which the orbiting masses reach the innermost stable circular orbit (ISCO), and Δt is the time-length of the $f_{\alpha}(t, \vec{\lambda})$ curve, which remains unchanged under scaling.

This construction allows us to probe harmonic content beyond the quadrupole mode. Setting $\alpha = 2$, we obtain the energy of the dominant quadrupole mode corresponding to $m = 2$, $S(\alpha)$ at $\alpha = 3$ represents the energy of the octupole mode $m = 3$, and so on. This strategy was proposed in Ref. [54] for the detection of higher-order modes in GW signals. In that work, scaling was applied to the (2,2) mode track, so the α values used there are half those used in our current analysis.

Instead of the conventional CWT based on the Gabor–Morlet wavelet [56], we employ the Synchroextracting Transform (SET) [57, 58] to obtain high-resolution time–frequency representations (TFRs) in our analysis. By “high resolution,” we refer to improved localization of signal energy in the time–frequency plane. The mathematical formulation of SET is provided in Appendix A,

where we also illustrate its advantage in constructing $S(\alpha)$. Accordingly, in our analysis, we replace $\tilde{X}(t, f)$ with $\text{SET}[\tilde{W}^w(t, f)]$ as defined in Eq. (A2).

B. Setup for Consistency Test

In our study, we consider two types of injections: a beyond-GR signal assuming a massive graviton, and an eccentric waveform obtained from numerical simulations, as discussed in Sec. III. The massive graviton injection is generated for a GW170608-like system with aligned spins, assuming a graviton mass of $m_g = 70.7 \times 10^{-23} \text{ eV}/c^2$. This value exceeds the upper bound reported for the GW170608 event by LVK [9], ensuring observable deviations from general relativity. A phenomenological modification to the GW dispersion relation is introduced by adding a power-law term in momentum to the GR dispersion relation $E^2 = p^2 c^2$, where E and p denote the energy and momentum of the GW, and c is the speed of light. The modified dispersion takes the form $E^2 = p^2 c^2 + A_{\gamma} p^{\gamma} c^{\gamma}$, where A_{γ} and γ are phenomenological parameters. The exponent γ can take values from 0 to 4 in increments of 0.5. The graviton mass is related to the A_0 case by $m_g = A_0^{1/2}/c^2$, where $A_0 > 0$ corresponds to a massive graviton, i.e., the dispersion relation for a massive particle in vacuum [59]. The waveform is generated using a phenomenological model that incorporates the effects of this dispersion into the GW phase evolution in the frequency domain. The correction to the phase, $\Phi(f)$, is given by $\delta\Phi(f) = -\pi c D_L / \lambda_g^2 f$, where $\lambda_g = h/(m_g c)$ is the Compton wavelength of the graviton, h is Planck’s constant, and D_L is the binary’s luminosity distance. We henceforth refer to this waveform as the “non-GR signal” and use it throughout to illustrate our methodology.

Throughout this work, we perform the injection studies assuming a network of three detectors – Hanford (H1), Livingston (L1), and Virgo (V1) – assuming their advanced designed sensitivities: **aLIGOZeroDetHighPower** for H1 and L1 [60], and **AdvVirgo** for V1 [61], as implemented in LALSUITE [62]. We perform injection analyses assuming a starting frequency of 20 Hz and the network SNR is set to ~ 43.5 .

We shall now describe our method in the steps discussed in the following. This method is also summarized by the flowchart in Fig. 1.

Step 1: We perform Bayesian parameter estimation of the GW signal $y(t)$ (here the non-GR signal) using the BILBY [63] package with DYNesty nested-sampling algorithm [64]. Throughout this work, we perform the analyses using the IMRPHENOMXP waveform model [65], which is a phenomenological approximant

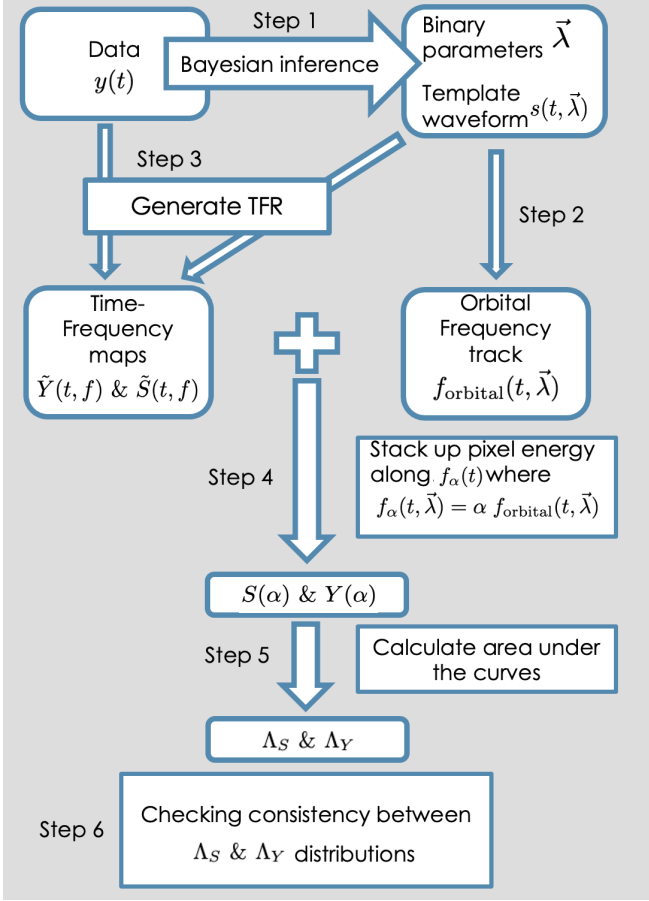


FIG. 1. Flowchart summarizing the steps of the Consistency test.

designed to describe the full inspiral-merger-ringdown (IMR) evolution of BBH coalescences incorporating the orbital precession effects. Within the framework of GR, IMRPHENOMXP provides an efficient and accurate representation of GW signals from precessing binaries assuming quasi-circular orbits. For the analyses, we consider uniform priors for chirp mass and mass ratio and power law priors for luminosity distance. For the rest of the parameters, we refer to Table 1 in Ref. [63] and implemented the default priors.

Step 2: We calculate the orbital frequency $f_{\text{orbital}}(t, \vec{\lambda})$ using the mass and spin information of the BHs from the posterior distributions of the BBH parameters $\vec{\lambda}$.

Step 3: It involves generating the TFRs. We first whiten the data $y(t)$ and template waveform $s(t, \vec{\lambda})$ using the detector's power spectral densities. We use Eq. (A2) to execute SET on $y(t)$ and obtain $\tilde{Y}(t, f)$. Similarly, $\tilde{S}(t, f)$ is the synchroextracted TF map of $s(t, \vec{\lambda})$.

Step 4: As discussed in subsection II A, we generate

the arbitrary frequency tracks $f_\alpha(t, \vec{\lambda})$ using Eq. (1). This allows us to gradually scroll the $f_{\text{orbital}}(t, \vec{\lambda})$ curve along the frequency direction in the TF plane by changing the value of α in small discrete steps between α_{\min} and α_{\max} . We stack up the pixel energy of $\tilde{Y}(t, f)$ using Eq. (2) and obtain $Y(\alpha)$. Similarly, we obtain $S(\alpha)$ using $\tilde{S}(t, f)$. Any disagreement between the data (here, the non-GR signal) $y(t)$ and the template waveform $s(t, \vec{\lambda})$ will propagate into the $S(\alpha)$ and $Y(\alpha)$ curves. Fig. 2 (left panel) shows the dissimilarity between the $S(\alpha)$ and $Y(\alpha)$ curves due to the massive graviton effect in the signal.

Step 5: The energy of the GW signals is well localized in both the $S(\alpha)$ and the $Y(\alpha)$ curves around $\alpha \approx 2$. We calculate the area under these curves around the peak corresponding to the quadrupole mode in the range $\alpha \in [1.6, 2.4]$ to quantify the shape heterogeneities between $S(\alpha)$ and $Y(\alpha)$. The area under the $Y(\alpha)$ curve is defined as,

$$\Lambda_Y = \int_{\alpha_{\min}}^{\alpha_{\max}} Y(\alpha) d\alpha. \quad (3)$$

We use the same equation to calculate Λ_S (area under the $S(\alpha)$ curve) by replacing $Y(\alpha)$ with $S(\alpha)$. We compute Λ_Y (Λ_S) in the above equation for a single detector. For a network of detectors, we obtain the combined value Λ_Y (Λ_S) by adding the individual values from each detector.

Step 6: We randomly choose a large number of posterior samples. Then, for each posterior sample, we repeat Step 2 to Step 5 to construct the Λ_S and Λ_Y distributions. Throughout this work, we use 1000 posterior samples for each case study. The distributions of Λ_Y and Λ_S are shown in Fig. 2 (right panel) along with their 95% intervals. If the theoretical waveform is consistent with the observed signal, we expect these two distributions to have significant overlap.

To determine the level of agreement between the observed signal and our waveforms, we calculate the distance (\mathcal{D}_S^Y) between these two distributions, which is defined as difference between the Λ_Y and average of Λ_S ,

$$\mathcal{D}_S^Y = |\Lambda_Y - \langle \Lambda_S \rangle| \quad (4)$$

We use the 1σ ($\sim 68\%$) width of the Λ_S distribution as the unit of distance measurement, which is denoted as σ_S . For the massive graviton injection, we find that $\langle \mathcal{D}_S^Y \rangle = 3.75 \sigma_S$, which means the Λ_Y distribution lies, on average, outside the 99.999% confidence interval

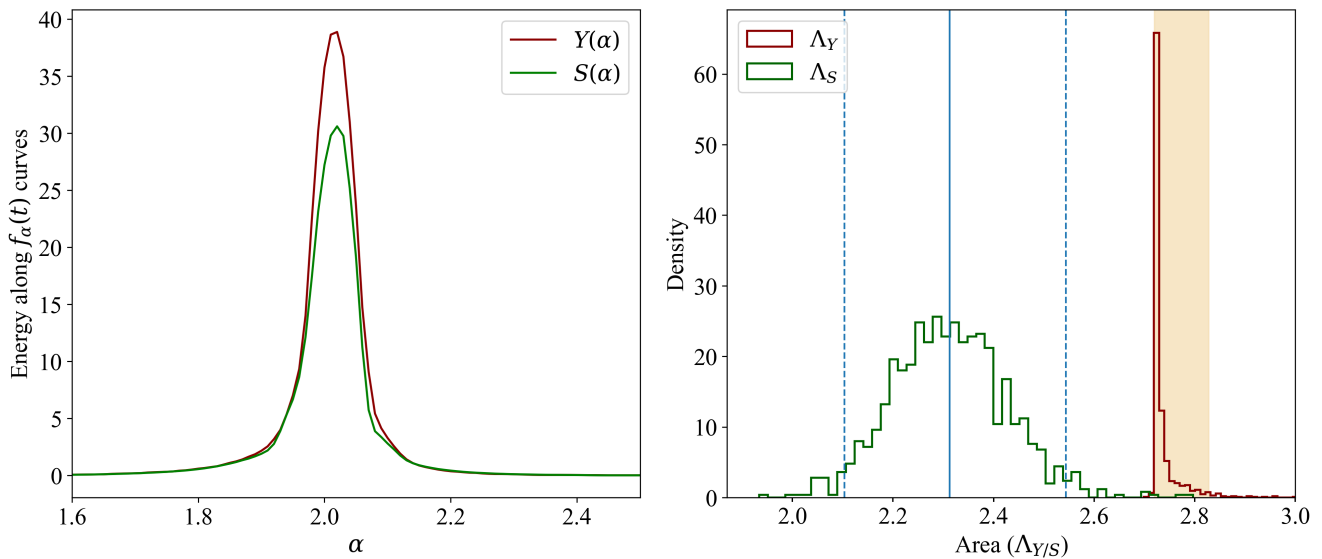


FIG. 2. (Left Panel) Template vector $S(\alpha)$ following GR theory for BBH system generated using the IMRPHEMOMXP waveform model and $Y(\alpha)$ vector following beyond-GR theory for the same BBH system. (Right Panel) Distributions of Λ_S (in green) and Λ_Y (in maroon) for the non-GR signal and recovered with IMRPHEMOMXP waveform model. The light beige shaded zones represent the respective 95% intervals of the Λ_Y distribution. 95 % intervals of the Λ_S distribution are marked by the vertical dashed blue lines and the mean of Λ_S distribution is marked by the solid blue vertical line.

of Λ_S distribution. In Fig. 2 (right panel) the visual evidence that the 2 distributions are well separated (95% intervals of the distributions do not overlap) is also justified by the distance calculation.

C. GR Background and Statistics

In this subsection, we construct a GR-based background as the reference framework to establish the validity of our consistency test. The astrophysical GW signals detected by the LIGO interferometers are embedded in the instrument noise. We replicate a similar scenario by generating several stationary Gaussian noise realizations weighted by the sensitivity curve of Advanced LIGO and Virgo detectors, as discussed in Sec. II B. We inject an identical GW signal generated using the IMRPHEMOMXP model in all noise realizations. To study how the presence of noise impacts our proposed analysis, we repeat the analysis of these noisy signals following the steps in Fig. 1.

Fig. 3 shows the distributions of the area under the α curves, Λ_Y and Λ_S for 10 noise realizations. The tag \mathcal{S}_N represents the serial number of the simulations used for the analysis. The distributions for all the noise realizations are displayed in Fig. 8 and Fig. 9 of Appendix B.

The summary of the distance calculation is displayed in Fig. 4. The range of the distance values for each of the IMRPHEMOMXP waveform injections in Gaussian

noise realizations is represented by grey error bars in Fig. 4. The averages of each distance are shown by the black plus labels. We have also put forward these values for the non-GR case, which we have discussed before, and the cases with additional physics, discussed in the following sections, in different color schemes. The distance calculations for these cases lie beyond the 3σ range, whereas for GR injection in the presence of noise, the distance estimates are well-constrained within the 3σ limit. Therefore, we claim that the presence of noise does not hamper our consistency test. Table I shows the corresponding numerical values.

III. CASE STUDY: ECCENTRIC BINARY SYSTEM

The three observational runs conducted by the LIGO Collaboration have reported 98 compact binary merger events. These signals are interpreted as mergers of quasicircular compact binaries, with no clear evidence for an eccentric compact binary system [4, 66]. With improved sensitivities of the detectors, the prospects of detecting eccentric binaries, particularly those formed in dense stellar environments such as globular clusters and galactic nuclei, are more promising in the ongoing O4 run and future observational runs [67].

The current widely used waveform models to explain the GW observations from BBH coalescences consider

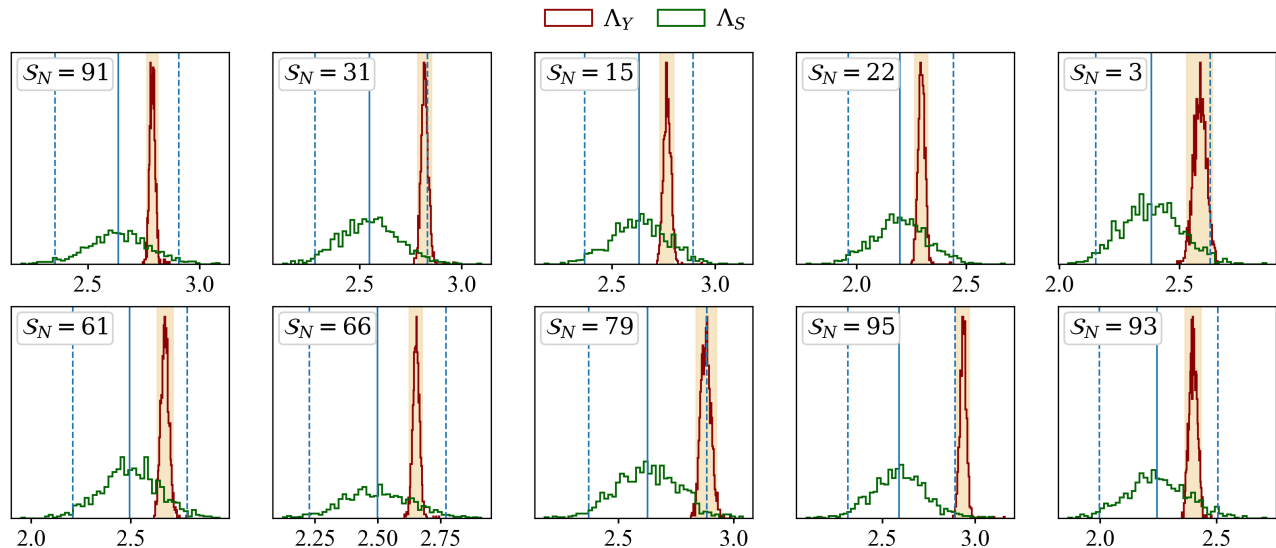


FIG. 3. Comparison between Λ_S (green) and Λ_Y (maroon) distributions is shown for an identical GR injection with ten different noise realizations. The quantity S_N in each panel represents the simulation number. The injection waveform was generated using the IMRPHENOMXP model and recovered with the same waveform model. The light beige shaded region represents the 95% interval of the Λ_Y distribution. The solid vertical line and the dashed vertical lines denote the mean and 95% interval of Λ_S distribution, respectively. We show this comparison for all the simulations in Fig. 8 and 9. We constructed these Λ_S and Λ_Y distributions using 1000 randomly selected posterior samples.

| Injection type | Average distance $\langle \mathcal{D}_S^Y \rangle / \sigma_S$ |
|--|---|
| GR injections with many noise realizations | [0.08, 2.37] |
| Massive graviton | 3.76 |
| Eccentric BBH | 5.84 |
| GW190814: (2,2) mode | 3.24 |
| GW190814: (2,2)+(3,3) modes | 2.14 |

TABLE I. The average distance $\langle \mathcal{D}_S^Y \rangle$ between the Λ_Y and Λ_S distributions is shown for three different types of injections: GR injections with many noise realizations, a non-GR signal with a massive graviton, and an eccentric BBH waveform, as discussed in Secs. II C, II B, and III, respectively. The values of $\langle \mathcal{D}_S^Y \rangle$ are marked with a ‘+’ symbol in Fig. 4.

quasi-circular orbits. Here, we investigate the efficiency of our method of consistency test to identify the missing physics, in the context of unmodeled eccentric orbit in GW waveform models.

We consider a numerical relativity (NR) waveform of an eccentric BBH (eBBH) system provided in the Simulating eXtreme Spacetimes (SXS) catalog. We specifically inject the SXS:BBH:1360 waveform, which was simulated for a non-spinning equal mass eccentric binary [68, 69]. As the eccentricity evolves with time, we report the reference

eccentricity $e_{\text{ref}} \sim 0.3636$ as measured at a reference orbital frequency of $Mf_0 = 0.0153$, and the reference mean anomaly $l_{\text{ref}} \sim 113.2^\circ$. In our analysis, we scale the simulation for a total mass of $60 M_\odot$, which is suitable for observing with 2nd generation detectors. So the reference eccentricity in this example corresponds to $f_0 \approx 50$ Hz.

Analyzing this eBBH signal in our methodological framework (following the steps in Fig. 1 for 1000 random samples) fetches some exciting results, which we discuss here. Fig. 5 (top panel) shows the TF representation generated by SET, and an eccentric higher-order mode is seen in addition to the dominant quadrupole mode. It becomes more evident as we evaluate the $Y(\alpha)$ and $S(\alpha)$ vectors (see Fig. 5 (Middle panel)). For this example, the calculation of the area under the α curves should not be restricted in the range $\alpha \in [1.6, 2.4]$ since all the energy in the TF plane is derived from the signal in the absence of noise. Distributions of the area under the $Y(\alpha)$ and $S(\alpha)$ curves, Λ_Y and Λ_S are displayed in Fig. 5 (bottom panel). In this case, as well, we note that the Λ_Y and Λ_S distributions are well separated.

Statistical evaluation of the effectiveness of our method while analyzing this eBBH system is recorded in Table I. The distance calculations for the eBBH case lie beyond the $3\sigma_S$ limit. It can be better visualized when demonstrated alongside the GR background in Fig. 4.

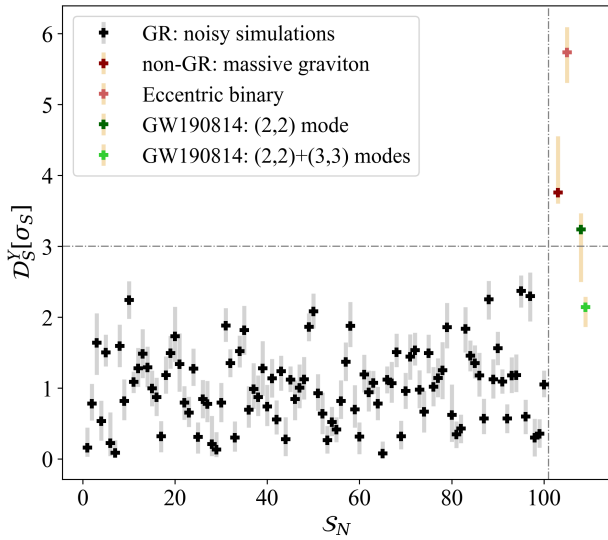


FIG. 4. The distance \mathcal{D}_S^Y between the Λ_Y and Λ_S distributions is shown for GR injections of quasi-circular binaries (black), a massive graviton non-GR injection (maroon), and an eccentric BBH injection (orange), all recovered using a quasi-circular GR waveform. Results for the GW190814 event are shown for two recovery cases: one using only the dominant quadrupole mode (dark green) and another including higher-order modes (light green). Since \mathcal{D}_S^Y is expressed in units of σ_S , it is not susceptible to the choice of the power spectral density for whitening the data and the posterior waveform. The median of each \mathcal{D}_S^Y distribution is marked by a ‘+’ symbol, with shaded vertical bands indicating the corresponding 95% credible intervals.

IV. ANALYZING GW190814 SIGNAL

To demonstrate the sensitivity of our testing framework for identifying missing physics with real data, we apply our method to the GW190814 event [53], assuming that the analyzing template waveform does not include higher-order modes. GW190814 is one of the exceptional events detected during the first half of the third observing run by the LVC Collaboration [53]. It was inferred that this signal was produced by the merger of a highly asymmetric binary with a mass ratio of approximately 9:1. This allowed us to find strong evidence of higher-order mode radiation in the GW. We investigate whether our method can indicate that a purely quadrupolar waveform is insufficient to represent the GW190814 signal. If so, what is the significance of the missing physics?

To analyze the GW190814 signal, we use the strain data released with the GWTC-2.1 catalog by LVC [70, 71]. In order to assess the effect of neglecting higher-order modes, we perform a parameter estimation using the IMRPHENOMXP model that incorporates only the

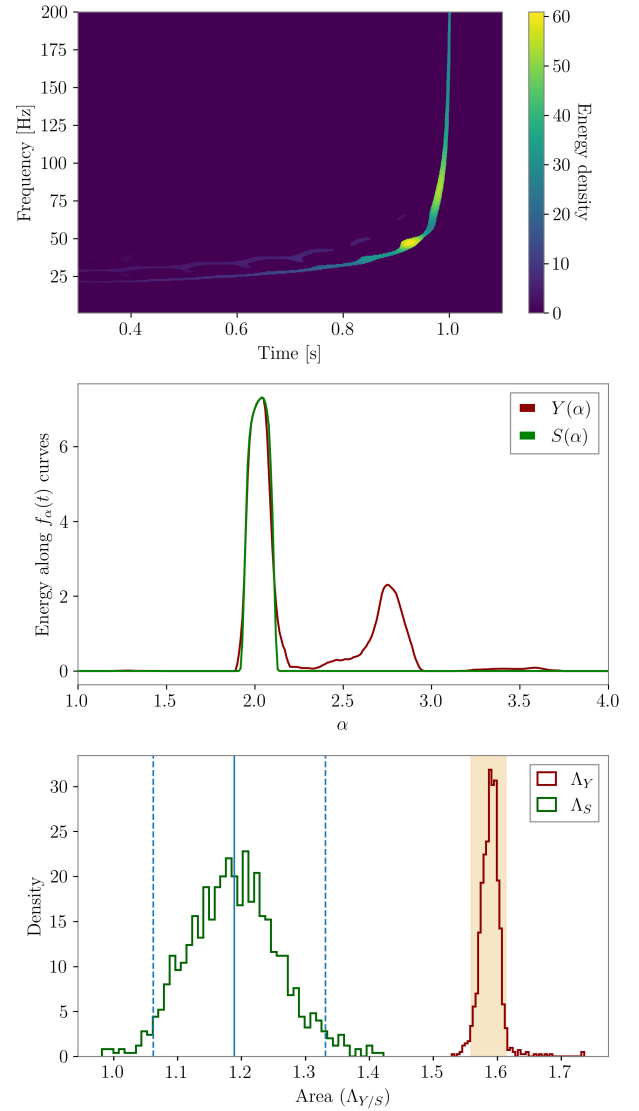


FIG. 5. Illustration of the results from the eccentric BBH injection analysis: the top panel shows the time-frequency map of the injected signal with SET; the middle panel shows the comparison between the injected signal $Y(\alpha)$ and the template waveform $S(\alpha)$; and the bottom panel shows the comparison between the Λ_S and Λ_Y distributions. The vertical dashed line indicates the 95% interval of the Λ_S distribution, and the shaded band represents the Λ_Y distribution.

dominant quadrupole mode. Using the IMRPHENOMXP posterior samples, we perform our new consistency test as described in Sec. II B and estimate the Λ_Y and Λ_S distributions. Fig. 6 shows the comparison Λ_Y and Λ_S distributions, 95% intervals of these distributions are well separated. We also compute the distance between these two distributions $\langle \mathcal{D}_S^Y \rangle = 3.24 \sigma_S$ as highlighted in Fig. 4, which is above the 3σ level. This implies that the quadrupolar waveform model IMRPHENOMXP is

inadequate to represent the GW190814 signal.

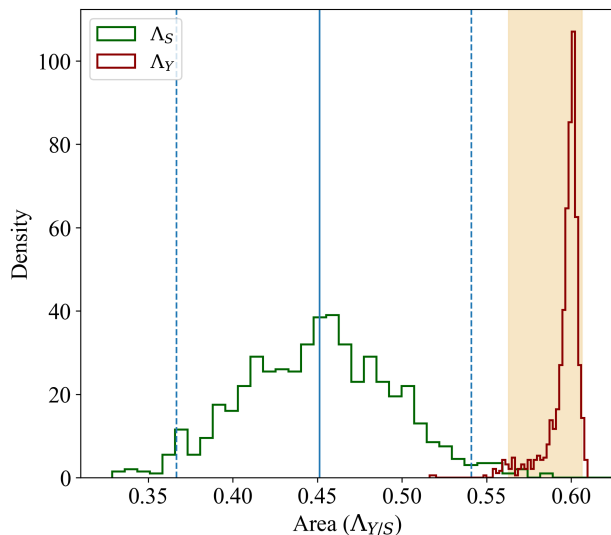


FIG. 6. Illustration of GW190814 results when the signal is analyzed with the IMRPHENOMXP waveform model. The distributions of Λ_S and Λ_Y —defined as the areas under the $S(\alpha)$ and $Y(\alpha)$ curves, respectively—are shown in green and maroon. The blue dashed lines represent the 95% credible interval for the Λ_S distribution, with the corresponding median indicated by a solid vertical line. The light maroon shaded region denotes the 95% credible interval of the Λ_Y distribution.

On the other hand, we redo the entire analysis using the publicly released IMRPHENOMXPHM posteriors [71] to reconstruct the waveform that includes the dominant quadrupole mode along with the subdominant modes. The Λ_Y and Λ_S distributions obtained in this leg of the analysis show significant overlap and $\langle \mathcal{D}_S^Y \rangle = 2.14 \sigma_S$. These distance estimates are also plotted in Fig. 4 along with the GR-based background.

When only the quadrupole mode is included, the reconstructed waveform and TFR show noticeable deviations from the theoretical expectations. These deviations are due to the expected impact of higher-order multipoles, which become significant for systems with high mass ratios, such as this event or GW190412. The lack of subdominant modes results in an incomplete representation of the GW signal, leading to systematic biases in the frequency evolution. For GW190412 event, we found the Λ_Y and Λ_S distributions show $\langle \mathcal{D}_S^Y \rangle = 1.42 \sigma_S$ and $1.06 \sigma_S$ for IMRPHENOMXP and IMRPHENOMXPHM waveform models. Including subdominant modes captures additional waveform features that are otherwise missed. Our results reveal a distinct improvement in the agreement between the data and the theoretical model when all modes are incorporated into the waveform model.

V. DISCUSSION

In this study, we introduced a novel consistency test designed to evaluate the validity of GR in describing the orbital frequency evolution of the BBH systems by analyzing GW signals in the time-frequency domain. Our method leverages high-resolution SET spectrograms, stacking pixel energies along the GR-predicted orbital frequency trajectory. Deviations from GR manifest as distortions in the time-frequency energy distribution, which we quantify by measuring the distance between the energy profiles derived from observational data and those predicted by our search waveform models.

We demonstrated the sensitivity of this approach through various test cases, including signals with non-GR features introduced by a massive graviton in a GW170608-like BBH system. The results confirm that our method can detect such deviations, offering a model-agnostic tool for probing the inspiral dynamics of compact binaries.

Our framework also shows promise in identifying missing physical effects in the baseline GR waveform model. For instance, when applied to signals from eccentric BBH systems, while the search template waveform was assumed to be a quasi-circular orbit during Bayesian inference, our test detected significant discrepancies. Finally, in the analysis of GW190814 using both the IMRPHENOMXP and IMRPHENOMXPHM waveform models, our method successfully revealed that the missing higher-order modes in the IMRPHENOMXP model could not explain the GW190814 signal. This demonstrates the utility of our approach in examining waveform fidelity.

By enabling precise tracking of orbital frequency evolution, this method has an enhanced sensitivity while testing longer chirp signals. As detector sensitivities improve and the event catalog expands, our approach offers a probe to additional physics in the upcoming observations, which shall include a variety of compact binaries. Analyzing more events lays the groundwork for detecting subtle imprints of new physics and motivation to further refine the waveform models.

ACKNOWLEDGMENTS

We are grateful to Haris M. K. and Justin Janquart for useful comments on our draft. This work was supported by the National Natural Science Foundation of China (NSFC), Grant No. 12250610185 and 12261131497, and the Natural Science Foundation of Shanghai, Grant No. 22ZR1403400. D. D. also acknowledges support from the China Scholarship Council (CSC), Grant No.

2022GXZ005434. S.R. is supported by the Fonds de la Recherche Scientifique - FNRS (Belgium). D. D. thanks Université catholique de Louvain for hospitality and support. The manuscript is based upon work supported by NSF's LIGO Laboratory, which is a major facility fully funded by the National Science Foundation (NSF), as well as the Science and Technology Facilities Council (STFC) of the United Kingdom, the Max-Planck-Society (MPS), and the State of Niedersachsen/Germany for support of the construction of Advanced LIGO and construction and operation of the GEO600 detector. Additional support for Advanced LIGO was provided by the Australian Research Council. Virgo is funded through the European Gravitational Observatory (EGO), by the French Centre National de Recherche Scientifique (CNRS), the Italian Istituto Nazionale di Fisica Nucleare (INFN) and the Dutch Nikhef, with contributions by institutions from Belgium, Germany, Greece, Hungary, Ireland, Japan, Monaco, Poland, Portugal, Spain. KAGRA is supported by the Ministry of Education, Culture, Sports, Science and Technology (MEXT), Japan Society for the Promotion of Science (JSPS) in Japan; National Research Foundation (NRF) and the Ministry of Science and ICT (MSIT) in Korea; Academia Sinica (AS) and National Science and Technology Council (NSTC) in Taiwan. We have used NUMPY [72], SCIPY [73], MATPLOTLIB [74] for analyses and preparing the figures in the manuscript.

Appendix A: Synchroextraction Transform (SET)

Time-frequency (TF) spectrograms very easily perceive the frequency evolution of BBH systems. However, most of the conventionally used TF methods encounter the problem of signal energy leakage to neighboring pixels, causing smudged patches in the TF plane. This is referred to as the Gabor inequality in literature [75]. We address this issue using a recently developed synchroextraction transform (SET) based on reassignment methods [57, 58]. The high-resolution TFR localizes the signal energy within a fewer number of pixels. Therefore, synchroextracted TF maps aid our requirement to detect the slightest changes in the frequency evolution resulting from beyond GR theories in contrast with the GR predicted frequency evolution of the BBH systems.

The primary concept of SET is to retain/extract the TF information of CWT most related to time-varying features of the GW signal, hence resulting in the removal of most of the smeared TF energy. For an accurate localization of the signal energy in the TF plane, SET involves the estimation of the instantaneous frequency, $\hat{f}(t, f)$. This approach to calculate $\hat{f}(t, f)$ is very efficient even in the

presence of noise.

$$\hat{f}(t, f) = f + \frac{i}{2\pi} \frac{\tilde{W}^{w'}(t, f)}{\tilde{W}^w(t, f)} \quad (\text{A1})$$

Here, $\tilde{W}^w(t, f)$ and $\tilde{W}^{w'}(t, f)$ are the CWTs of the GW signals taken with a Gabor-Morlet wavelet (w) and time derivative of Gabor-Morlet wavelet (w'). For the given definition of instantaneous frequency in Eq. (A1), the SET can be written as

$$\begin{aligned} \text{SET}[\tilde{W}^w(t, f)] &= \int \tilde{W}^w(t, f) \delta(f - \hat{f}(t, f)) df \quad (\text{A2}) \\ &= \int \tilde{W}^w(t, f) \delta\left(-\frac{i}{2\pi} \frac{\tilde{W}^{w'}(t, f)}{\tilde{W}^w(t, f)}\right) df \quad (\text{A3}) \end{aligned}$$

Fig. 7 shows the spectrograms corresponding to $\tilde{W}^w(t, f)$ and $\text{SET}[\tilde{W}^w(t, f)]$ for a (30, 30) M_\odot BBH system. The Advanced LIGO and Virgo power spectral densities are used to whiten the GW strain. We note that the (2,2) mode energy is very highly localized in fewer pixels in the $\text{SET}[\tilde{W}^w(t, f)]$ spectrogram. The $S(\alpha)$ vectors also show a much narrower peak at $\alpha \approx 2$ for the SET compared to the peak for the CWT spectrogram.

Appendix B: Injection study

To demonstrate the statistical validation of our consistency test, we use 100 IMRPHENOMXP injections in Gaussian noise realizations as our signal and compute the Λ_Y and Λ_S distribution for these noisy injections. We provide a visual summary of all the noisy realizations in Fig. 8 and Fig. 9. Out of these, 10 randomly selected sets of distributions were displayed earlier in Fig. 3. Hence, we develop a GR-based background within the framework of the second-generation GW interferometric detectors.

We can see that Λ_S and Λ_Y have some differences. This is an intrinsic feature that comes from the noise contribution in TF pixels that are used to generate Λ_Y , whereas Λ_S does not have any noise contribution.

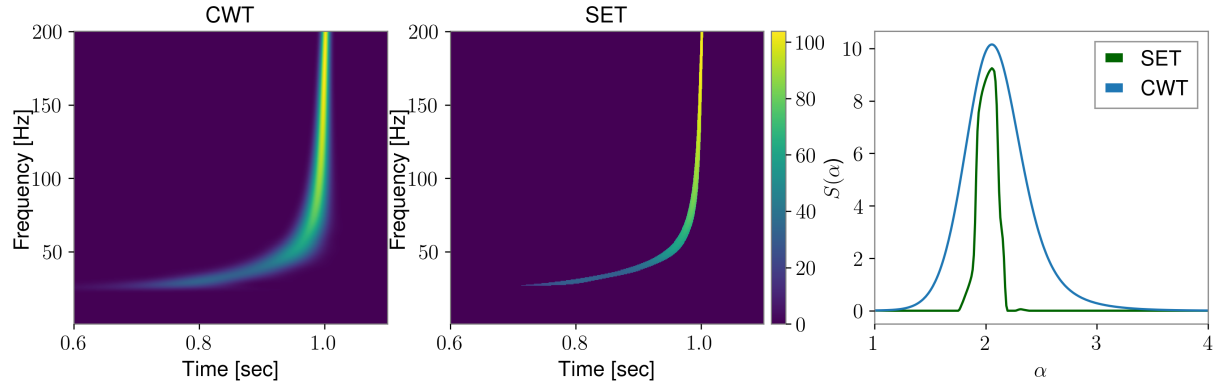


FIG. 7. Comparison between the CWT (left panel) and SET (middle panel) of a $(30, 30) M_{\odot}$ BBH waveform generated using the IMRPHENOMXP model, along with their respective $S(\alpha)$ curves shown in the right panel. SET results in better TF resolution, which translates to better resolution in α . Good resolution in α is very important to make the statistics work efficiently for our project.

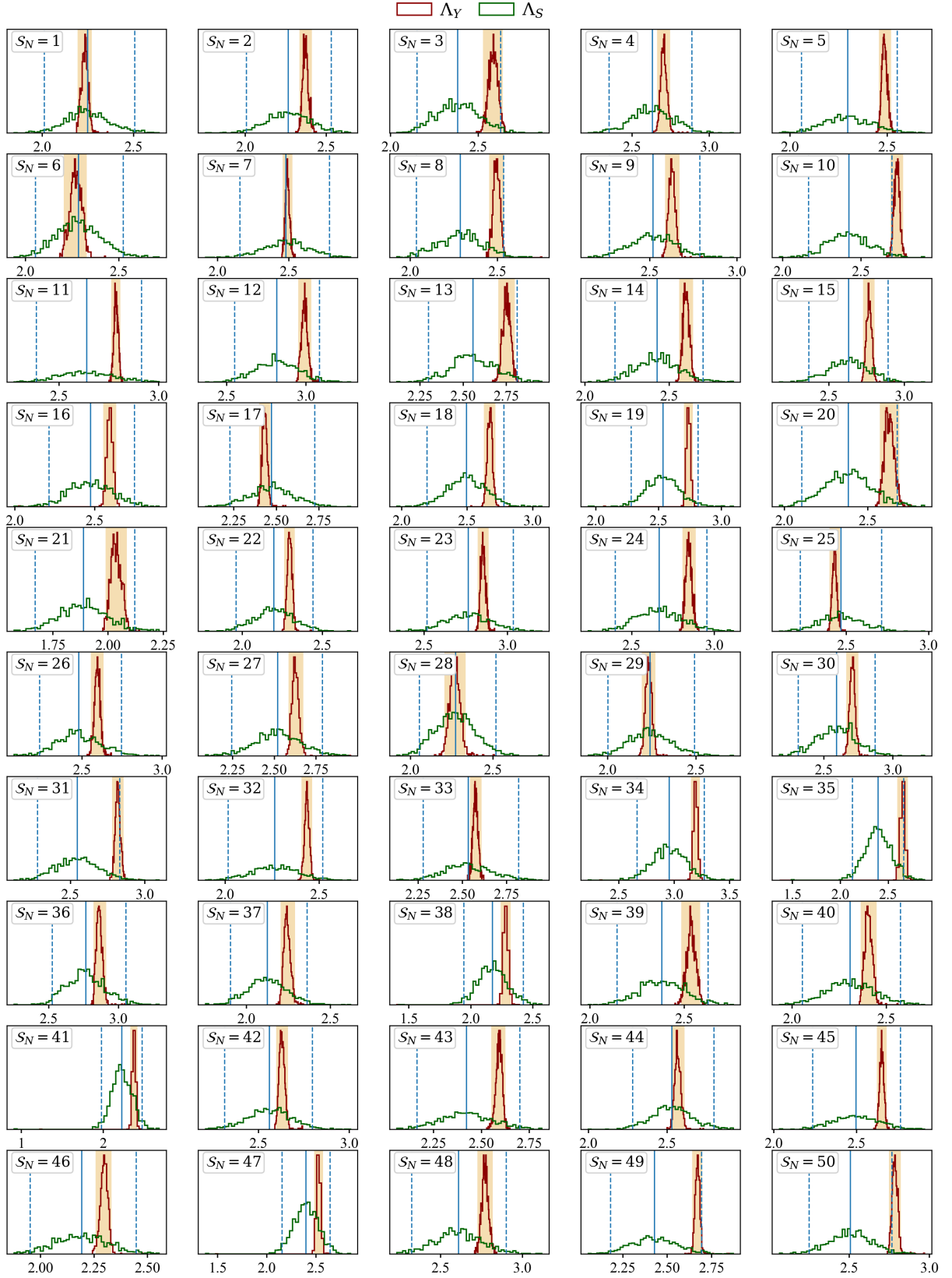


FIG. 8. Same as Fig. 3, but displaying the comparison between Λ_S and Λ_Y distributions for 50 simulations ($S_N = 1$ to 50). It is evident that 95% interval of Λ_S has at least a nominal overlap with the 95% interval of Λ_Y .

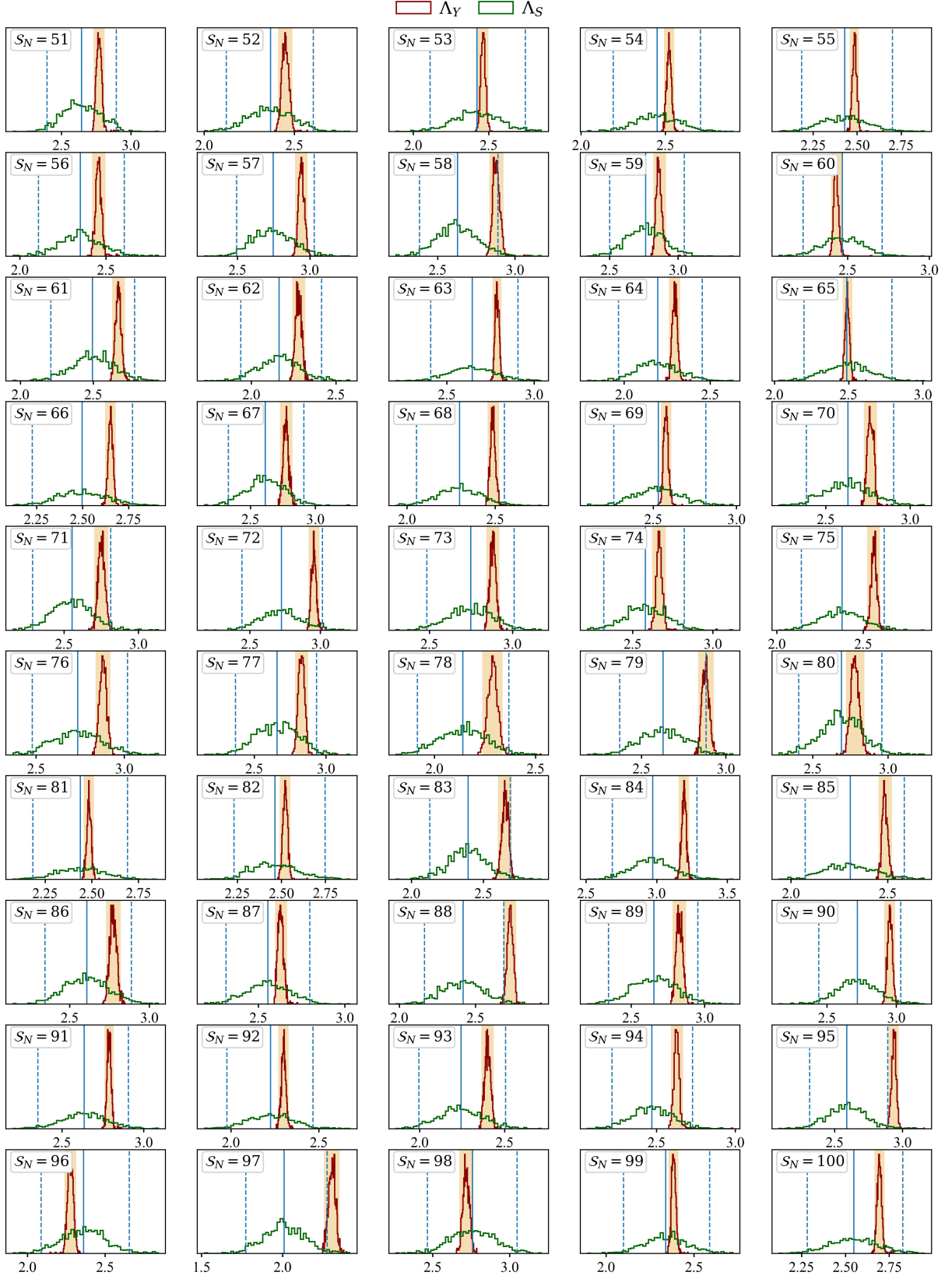


FIG. 9. Same as Fig. 3, but displaying the comparison between Λ_S and Λ_Y distributions for next 50 simulations ($S_N = 51$ to 100). It is evident that 95% interval of Λ_S has at least a nominal overlap with the 95% interval of Λ_Y .

-
- [1] B. P. Abbott *et al.* (LIGO Scientific, Virgo), “Observation of Gravitational Waves from a Binary Black Hole Merger,” *Phys. Rev. Lett.* **116**, 061102 (2016), [arXiv:1602.03837 \[gr-qc\]](#).
- [2] B. P. Abbott *et al.* (LIGO Scientific, Virgo), “GWTC-1: A Gravitational-Wave Transient Catalog of Compact Binary Mergers Observed by LIGO and Virgo during the First and Second Observing Runs,” *Phys. Rev. X* **9**, 031040 (2019), [arXiv:1811.12907 \[astro-ph.HE\]](#).
- [3] R. Abbott *et al.* (LIGO Scientific, Virgo), “GWTC-2: Compact Binary Coalescences Observed by LIGO and Virgo During the First Half of the Third Observing Run,” *Phys. Rev. X* **11**, 021053 (2021), [arXiv:2010.14527 \[gr-qc\]](#).
- [4] R. Abbott *et al.* (KAGRA, VIRGO, LIGO Scientific), “GWTC-3: Compact Binary Coalescences Observed by LIGO and Virgo during the Second Part of the Third Observing Run,” *Phys. Rev. X* **13**, 041039 (2023), [arXiv:2111.03606 \[gr-qc\]](#).
- [5] J. Aasi *et al.* (LIGO Scientific), “Advanced LIGO,” *Class. Quant. Grav.* **32**, 074001 (2015), [arXiv:1411.4547 \[gr-qc\]](#).
- [6] F. Acernese *et al.* (VIRGO), “Advanced Virgo: a second-generation interferometric gravitational wave detector,” *Class. Quant. Grav.* **32**, 024001 (2015), [arXiv:1408.3978 \[gr-qc\]](#).
- [7] B. P. Abbott *et al.* (LIGO Scientific, Virgo), “Tests of general relativity with GW150914,” *Phys. Rev. Lett.* **116**, 221101 (2016), [Erratum: *Phys. Rev. Lett.* **121**, 129902 (2018)], [arXiv:1602.03841 \[gr-qc\]](#).
- [8] B. P. Abbott *et al.* (LIGO Scientific, Virgo), “Tests of General Relativity with GW170817,” *Phys. Rev. Lett.* **123**, 011102 (2019), [arXiv:1811.00364 \[gr-qc\]](#).
- [9] B. P. Abbott *et al.* (LIGO Scientific, Virgo), “Tests of General Relativity with the Binary Black Hole Signals from the LIGO-Virgo Catalog GWTC-1,” *Phys. Rev. D* **100**, 104036 (2019), [arXiv:1903.04467 \[gr-qc\]](#).
- [10] R. Abbott *et al.* (LIGO Scientific, Virgo), “Tests of general relativity with binary black holes from the second LIGO-Virgo gravitational-wave transient catalog,” *Phys. Rev. D* **103**, 122002 (2021), [arXiv:2010.14529 \[gr-qc\]](#).
- [11] R. Abbott *et al.* (LIGO Scientific, VIRGO, KAGRA), “Tests of General Relativity with GWTC-3,” (2021), [arXiv:2112.06861 \[gr-qc\]](#).
- [12] Cosimo Bambi, *Black Holes: A Laboratory for Testing Strong Gravity* (Springer, 2017).
- [13] Nicolas Yunes and Frans Pretorius, “Dynamical Chern-Simons Modified Gravity. I. Spinning Black Holes in the Slow-Rotation Approximation,” *Phys. Rev. D* **79**, 084043 (2009), [arXiv:0902.4669 \[gr-qc\]](#).
- [14] Burkhard Kleihaus, Jutta Kunz, and Eugen Radu, “Rotating Black Holes in Dilatonic Einstein-Gauss-Bonnet Theory,” *Phys. Rev. Lett.* **106**, 151104 (2011), [arXiv:1101.2868 \[gr-qc\]](#).
- [15] Niklas Becker, Laura Sagunski, Lukas Prinz, and Saeed Rastgoo, “Circularization versus eccentricification in intermediate mass ratio inspirals inside dark matter spikes,” *Phys. Rev. D* **105**, 063029 (2022), [arXiv:2112.09586 \[gr-qc\]](#).
- [16] Steven B. Giddings, “Astronomical tests for quantum black hole structure,” *Nature Astron.* **1**, 0067 (2017), [arXiv:1703.03387 \[gr-qc\]](#).
- [17] Ze-Yi Tu, Tao Zhu, and Anzhong Wang, “Periodic orbits and their gravitational wave radiations in a polymer black hole in loop quantum gravity,” *Phys. Rev. D* **108**, 024035 (2023), [arXiv:2304.14160 \[gr-qc\]](#).
- [18] Steven L. Liebling and Carlos Palenzuela, “Dynamical boson stars,” *Living Rev. Rel.* **26**, 1 (2023), [arXiv:1202.5809 \[gr-qc\]](#).
- [19] Nicolas Yunes and Frans Pretorius, “Fundamental Theoretical Bias in Gravitational Wave Astrophysics and the Parameterized Post-Einsteinian Framework,” *Phys. Rev. D* **80**, 122003 (2009), [arXiv:0909.3328 \[gr-qc\]](#).
- [20] K. G. Arun, Bala R. Iyer, M. S. S. Qusailah, and B. S. Sathyaprakash, “Testing post-Newtonian theory with gravitational wave observations,” *Class. Quant. Grav.* **23**, L37–L43 (2006), [arXiv:gr-qc/0604018](#).
- [21] Michalis Agathos, Walter Del Pozzo, Tjonnie G. F. Li, Chris Van Den Broeck, John Veitch, and Salvatore Vitale, “TIGER: A data analysis pipeline for testing the strong-field dynamics of general relativity with gravitational wave signals from coalescing compact binaries,” *Phys. Rev. D* **89**, 082001 (2014), [arXiv:1311.0420 \[gr-qc\]](#).
- [22] Soumen Roy, Maria Haney, Geraint Pratten, Peter T. H. Pang, and Chris Van Den Broeck, “An improved parametrized test of general relativity using the IMR-PhenomX waveform family: Including higher harmonics and precession,” [arXiv e-prints](#), [arXiv:2504.21147 \(2025\)](#), [arXiv:2504.21147 \[gr-qc\]](#).
- [23] Ajit Kumar Mehta, Alessandra Buonanno, Roberto Cotesta, Abhirup Ghosh, Noah Sennett, and Jan Steinhoff, “Tests of general relativity with gravitational-wave observations using a flexible theory-independent method,” *Phys. Rev. D* **107**, 044020 (2023), [arXiv:2203.13937 \[gr-qc\]](#).
- [24] N. V. Krishnendu, K. G. Arun, and Chandra Kant Mishra, “Testing the binary black hole nature of a compact binary coalescence,” *Phys. Rev. Lett.* **119**, 091101 (2017), [arXiv:1701.06318 \[gr-qc\]](#).
- [25] Anna Puecher, Chinmay Kalaghatgi, Soumen Roy, Yoshinta Setyawati, Ish Gupta, B. S. Sathyaprakash, and Chris Van Den Broeck, “Testing general relativity using higher-order modes of gravitational waves from binary black holes,” *Phys. Rev. D* **106**, 082003 (2022), [arXiv:2205.09062 \[gr-qc\]](#).
- [26] Parthapratim Mahapatra, “Octupolar test of general relativity,” *Phys. Rev. D* **109**, 024050 (2024), [arXiv:2306.04703 \[gr-qc\]](#).
- [27] Parthapratim Mahapatra and Shilpa Kastha, “Parametrized multipolar gravitational waveforms

- for testing general relativity: Amplitude corrections up to 2PN order,” *Phys. Rev. D* **109**, 084069 (2024), [arXiv:2311.04672 \[gr-qc\]](#).
- [28] Richard Brito, Alessandra Buonanno, and Vivien Raymond, “Black-hole Spectroscopy by Making Full Use of Gravitational-Wave Modeling,” *Phys. Rev. D* **98**, 084038 (2018), [arXiv:1805.00293 \[gr-qc\]](#).
- [29] Elisa Maggio, Hector O. Silva, Alessandra Buonanno, and Abhirup Ghosh, “Tests of general relativity in the nonlinear regime: A parametrized plunge-merger-ringdown gravitational waveform model,” *Phys. Rev. D* **108**, 024043 (2023), [arXiv:2212.09655 \[gr-qc\]](#).
- [30] Gregorio Carullo, Walter Del Pozzo, and John Veitch, “Observational Black Hole Spectroscopy: A time-domain multimode analysis of GW150914,” *Phys. Rev. D* **99**, 123029 (2019), [Erratum: *Phys. Rev. D* **100**, 089903 (2019)], [arXiv:1902.07527 \[gr-qc\]](#).
- [31] Maximiliano Isi, Matthew Giesler, Will M. Farr, Mark A. Scheel, and Saul A. Teukolsky, “Testing the no-hair theorem with GW150914,” *Phys. Rev. Lett.* **123**, 111102 (2019), [arXiv:1905.00869 \[gr-qc\]](#).
- [32] Parthaprati Mahapatra, Marc Favata, and K. G. Arun, “Testing general relativity via direct measurement of black hole kicks,” *Phys. Rev. D* **110**, 084041 (2024), [arXiv:2308.08319 \[gr-qc\]](#).
- [33] Christopher J. Moore, Eliot Finch, Riccardo Buscicchio, and Davide Gerosa, “Testing general relativity with gravitational-wave catalogs: The insidious nature of waveform systematics,” *iScience* **24**, 102577 (2021), [arXiv:2103.16486 \[gr-qc\]](#).
- [34] Qian Hu and John Veitch, “Accumulating Errors in Tests of General Relativity with Gravitational Waves: Overlapping Signals and Inaccurate Waveforms,” *Astrophys. J.* **945**, 103 (2023), [arXiv:2210.04769 \[gr-qc\]](#).
- [35] Peter T. H. Pang, Juan Calderón Bustillo, Yifan Wang, and Tjonnie G. F. Li, “Potential observations of false deviations from general relativity in gravitational wave signals from binary black holes,” *Phys. Rev. D* **98**, 024019 (2018), [arXiv:1802.03306 \[gr-qc\]](#).
- [36] Purnima Narayan, Nathan K. Johnson-McDaniel, and Anuradha Gupta, “Effect of ignoring eccentricity in testing general relativity with gravitational waves,” *Phys. Rev. D* **108**, 064003 (2023), [arXiv:2306.04068 \[gr-qc\]](#).
- [37] Pankaj Saini, Sajad A. Bhat, Marc Favata, and K. G. Arun, “Eccentricity-induced systematic error on parametrized tests of general relativity: Hierarchical Bayesian inference applied to a binary black hole population,” *Phys. Rev. D* **109**, 084056 (2024), [arXiv:2311.08033 \[gr-qc\]](#).
- [38] Rohit S. Chandramouli, Kaitlyn Prokup, Emanuele Berti, and Nicolás Yunes, “Systematic biases due to waveform mismodeling in parametrized post-Einsteinian tests of general relativity: The impact of neglecting spin precession and higher modes,” *Phys. Rev. D* **111**, 044026 (2025), [arXiv:2410.06254 \[gr-qc\]](#).
- [39] Neil J. Cornish and Tyson B. Littenberg, “BayesWave: Bayesian Inference for Gravitational Wave Bursts and Instrument Glitches,” *Class. Quant. Grav.* **32**, 135012 (2015), [arXiv:1410.3835 \[gr-qc\]](#).
- [40] Sudarshan Ghonge, Katerina Chatziioannou, James A. Clark, Tyson Littenberg, Margaret Millhouse, Laura Cadonati, and Neil Cornish, “Reconstructing gravitational wave signals from binary black hole mergers with minimal assumptions,” *Phys. Rev. D* **102**, 064056 (2020), [arXiv:2003.09456 \[gr-qc\]](#).
- [41] S. Klimenko, S. Mohanty, M. Rakhmanov, and G. Mitselmakher, “Constraint likelihood analysis for a network of gravitational wave detectors,” *Phys. Rev.* **72**, 122002 (2005), [arXiv:gr-qc/0508068 \[gr-qc\]](#).
- [42] S. Klimenko *et al.*, “Method for detection and reconstruction of gravitational wave transients with networks of advanced detectors,” *Phys. Rev. D* **93**, 042004 (2016), [arXiv:1511.05999 \[gr-qc\]](#).
- [43] Soumen Roy, “Nonorthogonal wavelet transformation for reconstructing gravitational wave signals,” *Phys. Rev. Res.* **4**, 033078 (2022), [arXiv:2201.01526 \[gr-qc\]](#).
- [44] Stephon Alexander, Evan McDonough, Robert Sims, and Nicolas Yunes, “Hidden-Sector Modifications to Gravitational Waves From Binary Inspirals,” *Class. Quant. Grav.* **35**, 235012 (2018), [arXiv:1808.05286 \[gr-qc\]](#).
- [45] J. M. Gerard and Y. Wiaux, “Gravitational dipole radiations from binary systems,” *Phys. Rev. D* **66**, 024040 (2002), [arXiv:gr-qc/0109062](#).
- [46] Manuela Campanelli, C. O. Lousto, and Y. Zlochower, “Spinning-black-hole binaries: The orbital hang up,” *Phys. Rev. D* **74**, 041501 (2006), [arXiv:gr-qc/0604012](#).
- [47] Vijay Varma, Leo C. Stein, and Davide Gerosa, “The binary black hole explorer: on-the-fly visualizations of precessing binary black holes,” *Class. Quant. Grav.* **36**, 095007 (2019), [arXiv:1811.06552 \[astro-ph.HE\]](#).
- [48] Theodoros A. Apostolatos, Curt Cutler, Gerald J. Sussman, and Kip S. Thorne, “Spin induced orbital precession and its modulation of the gravitational wave forms from merging binaries,” *Phys. Rev. D* **49**, 6274–6297 (1994).
- [49] Mark Hannam, Patricia Schmidt, Alejandro Bohé, Leïla Haegel, Sascha Husa, Frank Ohme, Geraint Pratten, and Michael Pürrer, “Simple Model of Complete Precessing Black-Hole-Binary Gravitational Waveforms,” *Phys. Rev. Lett.* **113**, 151101 (2014), [arXiv:1308.3271 \[gr-qc\]](#).
- [50] Enrico Barausse, Vitor Cardoso, and Paolo Pani, “Environmental Effects for Gravitational-wave Astrophysics,” *J. Phys. Conf. Ser.* **610**, 012044 (2015), [arXiv:1404.7140 \[astro-ph.CO\]](#).
- [51] Soumen Roy and Rodrigo Vicente, “Compact binary coalescences in dense gaseous environments can pose as ones in vacuum,” *Phys. Rev. D* **111**, 084037 (2025), [arXiv:2410.16388 \[gr-qc\]](#).
- [52] Giada Caneva Santoro, Soumen Roy, Rodrigo Vicente, Maria Haney, Ornella Juliana Piccinni, Walter Del Pozzo, and Mario Martinez, “First Constraints on Compact Binary Environments from LIGO-Virgo Data,” *Phys. Rev. Lett.* **132**, 251401 (2024), [arXiv:2309.05061 \[gr-qc\]](#).
- [53] R. Abbott *et al.* (LIGO Scientific, Virgo), “GW190814:

- Gravitational Waves from the Coalescence of a 23 Solar Mass Black Hole with a 2.6 Solar Mass Compact Object,” *Astrophys. J. Lett.* **896**, L44 (2020), [arXiv:2006.12611 \[astro-ph.HE\]](#).
- [54] Soumen Roy, Anand S. Sengupta, and K. G. Arun, “Unveiling the spectrum of inspiralling binary black holes,” *Phys. Rev. D* **103**, 064012 (2021), [arXiv:1910.04565 \[gr-qc\]](#).
- [55] R. Abbott *et al.* (LIGO Scientific, Virgo), “GW190412: Observation of a Binary-Black-Hole Coalescence with Asymmetric Masses,” *Phys. Rev. D* **102**, 043015 (2020), [arXiv:2004.08342 \[astro-ph.HE\]](#).
- [56] A. Grossmann and J. Morlet, “Decomposition of hardy functions into square integrable wavelets of constant shape,” *SIAM Journal on Mathematical Analysis* **15**, 723–736 (1984), <https://doi.org/10.1137/0515056>.
- [57] Gang Yu, Mingjin Yu, and Chuanyan Xu, “Synchroextracting transform,” *IEEE Transactions on Industrial Electronics* **64**, 8042–8054 (2017).
- [58] Duong-Hung Pham and Sylvain Meignen, “High-order synchrosqueezing transform for multicomponent signals analysis—with an application to gravitational-wave signal,” *IEEE Transactions on Signal Processing* **65**, 3168–3178 (2017).
- [59] Clifford M. Will, “Bounding the mass of the graviton using gravitational wave observations of inspiralling compact binaries,” *Phys. Rev. D* **57**, 2061–2068 (1998), [arXiv:gr-qc/9709011](#).
- [60] L. Barsotti, S. Gras, M. Evans, and P. Fritschel, *The updated Advanced LIGO design curve*, LIGO Technical Note T1800044-v5 (LIGO Scientific Collaboration, 2018) updated from T0900288-v3.
- [61] Alessandro Manzotti and Alexander Dietz, “Prospects for early localization of gravitational-wave signals from compact binary coalescences with advanced detectors,” *arXiv e-prints*, [arXiv:1202.4031](#) (2012), [arXiv:1202.4031 \[gr-qc\]](#).
- [62] LIGO Scientific Collaboration, “LIGO Algorithm Library - LALSuite,” free software (GPL) (2023).
- [63] Gregory Ashton *et al.*, “BILBY: A user-friendly Bayesian inference library for gravitational-wave astronomy,” *Astrophys. J. Suppl.* **241**, 27 (2019), [arXiv:1811.02042 \[astro-ph.IM\]](#).
- [64] Joshua S. Speagle, “Dynesty: a dynamic nested sampling package for estimating bayesian posteriors and evidences,” *Mon. Not. Roy. Astron. Soc.* **493**, 3132–3158 (2020), [arXiv:1904.02180 \[astro-ph.IM\]](#).
- [65] Geraint Pratten *et al.*, “Computationally efficient models for the dominant and subdominant harmonic modes of precessing binary black holes,” *Phys. Rev. D* **103**, 104056 (2021), [arXiv:2004.06503 \[gr-qc\]](#).
- [66] Ravikiran Hegde, Nirban Bose, and Archana Pai, “Probing eccentric higher-order modes through an effective chirp-mass model,” *Phys. Rev. D* **110**, 044026 (2024), [arXiv:2310.13662 \[gr-qc\]](#).
- [67] S. Soni, B. K. Berger, D. Davis, *et al.* (LIGO Scientific Collaboration), “LIGO Detector Characterization in the first half of the fourth Observing run,” (2024), [arXiv:2409.02831 \[astro-ph.IM\]](#).
- [68] Abdul H. Mroue *et al.*, “Catalog of 174 Binary Black Hole Simulations for Gravitational Wave Astronomy,” *Phys. Rev. Lett.* **111**, 241104 (2013), [arXiv:1304.6077 \[gr-qc\]](#).
- [69] Michael Boyle *et al.*, “The SXS Collaboration catalog of binary black hole simulations,” *Class. Quant. Grav.* **36**, 195006 (2019), [arXiv:1904.04831 \[gr-qc\]](#).
- [70] R. Abbott *et al.* (LIGO Scientific, VIRGO), “GWTC-2.1: Deep extended catalog of compact binary coalescences observed by LIGO and Virgo during the first half of the third observing run,” *Phys. Rev. D* **109**, 022001 (2024), [arXiv:2108.01045 \[gr-qc\]](#).
- [71] R. Abbott *et al.* (KAGRA, VIRGO, LIGO Scientific), “Open Data from the Third Observing Run of LIGO, Virgo, KAGRA, and GEO,” *Astrophys. J. Suppl.* **267**, 29 (2023), [arXiv:2302.03676 \[gr-qc\]](#).
- [72] Charles R. Harris *et al.*, “Array programming with NumPy,” *Nature* **585**, 357–362 (2020), [arXiv:2006.10256 \[cs.MS\]](#).
- [73] Pauli Virtanen *et al.*, “SciPy 1.0—Fundamental Algorithms for Scientific Computing in Python,” *Nat. Meth.* **17**, 261 (2020), [arXiv:1907.10121 \[cs.MS\]](#).
- [74] John D. Hunter, “Matplotlib: A 2D Graphics Environment,” *Comput. Sci. Eng.* **9**, 90–95 (2007).
- [75] Dennis Gabor, “Theory of communication. Part 1: The analysis of information,” *Journal of the Institution of Electrical Engineers-Part III: Radio and Communication Engineering* **93**, 429–441 (1946).